IEEE Access
Multidisciplinary | Rapid Review | Open Access Journal

Received 12 March 2024, accepted 16 April 2024, date of publication 29 April 2024, date of current version 8 May 2024.

Digital Object Identifier 10.1109/ACCESS.2024.3394698

RESEARCH ARTICLE

A Metasurface-Enhanced Substrate-Integrated Waveguide Antenna

JAVIER CHOCARRO[1], (Student Member, IEEE), JOSÉ MANUEL PÉREZ-ESCUDERO[1,2], JORGE TENIENTE[1,2], JUAN CARLOS IRIARTE-GALARREGUI[1,2], AND IÑIGO EDERRA[1,2], (Member, IEEE)

[1]Antenna Group, Department of Electrical, Electronic and Communications Engineering, Universidad Pública de Navarra (UPNA), 31006 Pamplona, Spain
[2]Institute of Smart Cities, Universidad Pública de Navarra (UPNA), 31006 Pamplona, Spain

Corresponding author: Iñigo Ederra (inigo.ederra@unavarra.es)

This work was supported in part by the Spanish State Research Agency under Project PID2019-109984RBC43/AEI/10.13039/501100011033, in part by the Universidad Pública de Navarra under Project PRO-UPNA11893, and in part by the Pre-Doctoral Scholarship Program. Open Access provided by Universidad Pública de Navarra.

ABSTRACT The design, manufacture and characterization of a slotted waveguide antenna using substrate-integrated waveguide (SIW) technology combined with a metasurface are described in this paper. The inclusion of the metasurface serves to augment the radiating aperture and narrows the E-plane cut of the antenna pattern, a characteristic that would otherwise be dictated by the slots. For demonstration, an 8-element slotted SIW (S-SIW) antenna array with a −20 dB sidelobe level Chebyshev distribution was designed and its performance was compared to that of a conventional slotted SIW array. Owing to the metasurface, the radiation pattern E-plane narrows and 3 dB gain improvement has been achieved, while keeping matching unaffected.

INDEX TERMS Metasurface, substrate integrated waveguide, slotted antenna.

I. INTRODUCTION

The antenna field is constantly developing, driven by the demanding specifications of new communication systems [1]. In particular, higher frequencies are required and alternatives to metallic waveguide-based configurations are being explored [2]. Substrate-integrated waveguides (SIW) have become an attractive solution, since they allow for the design of compact low-profile antennas that are relatively easy to manufacture and have moderate losses [3]. This technology has been employed e.g. in large arrays with linear [4] and circular polarizations [5].

Another solution for improving antenna performance is facilitated by the use of metamaterials [6]. The success of these periodic structures in recent years has led to an expansion of their use in antennas. As a result, communication antennas based on metasurfaces (MTS), planar versions of metamaterials, have become an alternative [1]. The benefits that MTSs bring to the antenna domain encompass various aspects [6], [7], [8], [9], [10]: miniaturization, radiation performance enhancement, e.g. gain or scanning performance, mutual coupling mitigation and volume reduction. These improvements extend to diverse applications beyond communications, such as sensing [11] or imaging [12]. In addition, taking advantage of the metamaterial implementation of the artificial magnetic conductor (AMC) concept, novel waveguiding configurations have emerged, such as gap-waveguides [13] or glide-symmetry-based waveguides [14].

Recently, metasurfaces have found a great development and various versions can be found in the literature, from impedance-modulated [8], [15] to Huygens' metasurfaces [9], [16]. One of their advantages is that a single feeding point can be used to illuminate an aperture, owing to the waves excited at the MTS-air interface. In this context, we propose the use of an MTS fed by a slotted waveguide antenna, so that the MTS allows tailoring the radiation in the antenna E-plane, where the pattern of standard slotted waveguide antennas is determined by the slot pattern. In addition, we will apply this concept to an SIW-based slotted waveguide, so that both the base antenna

The associate editor coordinating the review of this manuscript and approving it for publication was Hassan Tariq Chattha.

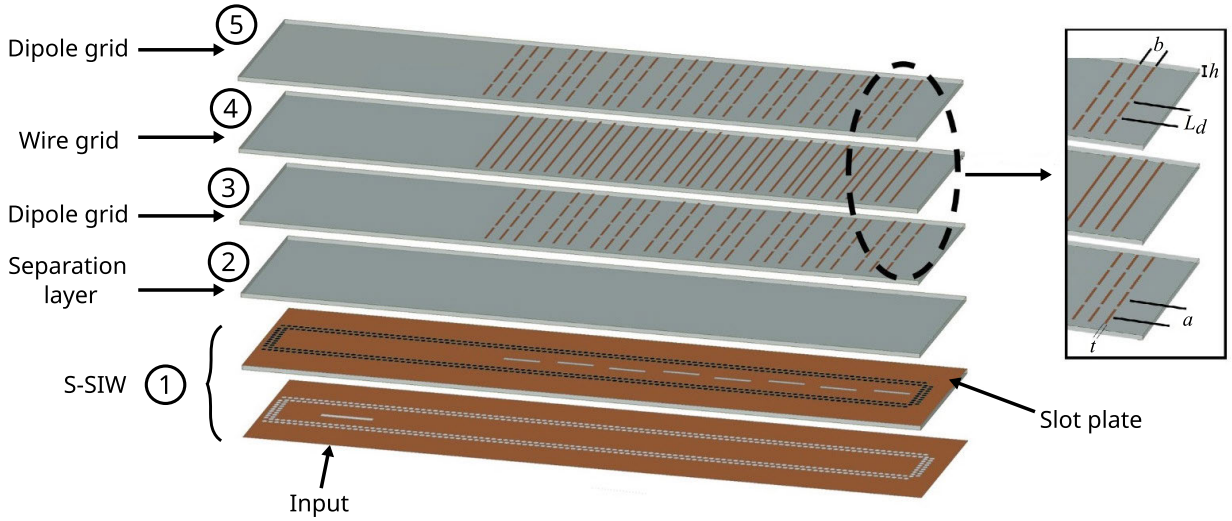

FIGURE 1. Exploded view of the proposed antenna. The inset shows in detail the metasurface and its main parameters. The main dimensions of the SIW are detailed in Section II. The dimensions of the metasurface are gathered in Table 1. Table 2 lists the dimensions and positions of the slots.

and MTS are created using the same dielectric substrate in a multilayer configuration. Other alternatives such as lenses or superstrates could be used to improve the performance of this type of antenna, but lenses are bulky and require placement at the focal length distance; similarly, the use of a superstrate would also increase the antenna profile with respect to using a metasurface.

Covering a slotted waveguide has been proposed as a means to improve its performance. First, a dielectric cover can be used as a radome [17], [18], [19], [20], [21], [22], [23], providing protection for the waveguide and preventing contamination through the slots. In addition, if properly designed, a Fabry-Perot cavity can be created to enhance the radiation pattern [22]. Likewise, patches [23] can be printed on the dielectric, which reduces the slot admittance. Finally, in [24] one-dimensional subwavelength periodic corrugated grooves were integrated on the top surface of an antenna, thereby reducing the radiation pattern beamwidth.

This study focuses on a slotted SIW antenna, which provides a performance similar to that of a slotted rectangular waveguide antenna in a low-profile configuration. In the literature we can find several examples in which superstrates are used to improve their performance. In [25], an array of patches was fed using an SIW slot array. In addition, different metamaterials have been used in combination with this type of antenna to achieve various objectives. An electric-inductive-capacitive (ELC) metasurface was proposed in [26] to reduce the coupling between slots in slotted SIW arrays and to improve their scanning capabilities. Coupling reduction has also been achieved in an MTS-assisted sparse array [27], where a gain increase of the order of 6 dB without sacrificing bandwidth was reported. However, the emphasis was placed on sparcification and limited improvement of the radiation pattern in the E-plane was achieved. For beam-direction control, an MTS was integrated with a slotted SIW array in [28]. In this case, the MTS, which combined Jerusalem crosses with a wireframe, acted as a lens and had to be placed at a certain distance from the radiating slots, which complicated the assembly. A similar approach can be found in [29], where the MTS lens was placed at $3\lambda_0$ from the slot antenna. Finally, in [30], an MTS allowed steering of the beam of a radial-line slot antenna array, whereas in [31] it served to reduce the antenna Radar Cross-Section (RCS).

If a single slot is considered, gain increase thanks to the use of an MTS has been demonstrated [32]. Polarization improvements can also be achieved, as shown in [33], where a cross-circular loop resonator MTS was used, and in [34], which proposed a MTS for polarization conversion and circular polarization generation. Finally, a metamaterial coating [35] that features epsilon-near-zero (ENZ) performance was used on top of an SIW-fed slot. In this case, the volumetric nature of the metamaterial does not fit a simple multilayer manufacturing approach.

In this study, we propose the use of a metasurface that improves the radiation properties of a slotted antenna in SIW technology (S-SIW) while maintaining a multilayer configuration. This multilayer approach simplifies manufacturing and provides advantages in terms of robustness and compactness with respect to the aforementioned configurations [27], [35]. The employed metasurface is described in [36], and consists of two layers of dipoles and another layer of wires between them, see Fig. 1. This metasurface has been used in previous works to improve the radiation performance of dipoles [37], [38], reduce mutual coupling between dipoles [38] and in rectangular-waveguide-based slotted waveguide antennas (SWA) [39]. In these previous studies, we achieved a gain increase of approximately 4 dB with respect to a conventional SWA antenna, while

maintaining the same bandwidth. In this case we adapted the metasurface to a low-profile solution based on an SIW antenna, which is compatible with multilayer PCB fabrication processes. This work builds upon and extends the preliminary results presented in [40], in which the concept was outlined. The main novelties as compared to these previous results include the following: (i) design of the transition to the feeding waveguide; (ii) design and numerical results for the complete antenna (including the transition from rectangular waveguide to SIW); (iii) fabrication of the antenna prototype; (iv) experimental verification of the antenna performance; and (v) post-measurement analysis and numerical simulations for the adjustment of the losses in the dielectric substrate and the antenna characterization.

The proposed solution is a straightforward alternative for tailoring the E-plane pattern compared to using an array. Even though in both cases there is an unavoidable size increase, our approach eliminates the need for an additional feeding network, since the MTS is directly fed by the slotted SIW, reaching a similar performance [41].

II. SUBSTRATE-INTEGRATED WAVEGUIDE DESIGN

A. SUBSTRATE-INTEGRATED WAVEGUIDE DIMENSIONS

In this study, a metasurface is used to enhance the radiation properties of an S-SIW antenna. Similar to standard rectangular waveguide slotted antennas, this antenna is formed by creating longitudinal slots in one of the ground planes of a SIW.

The SIW parameters were calculated following the expressions in [42]. Starting from the corresponding standard rectangular waveguide, WR34 for operation around 24 GHz, the required width of a Rogers RT5880 ($\epsilon_r = 2.2$) filled rectangular waveguide would be: $a_d = a/\sqrt{\epsilon_r} = 5.82$ mm, where $a = 8.635$ mm is the width of a WR34 waveguide.

The equivalent width of the SIW, a_s, can be related to the dielectric-filled rectangular waveguide width, a_d, and the SIW parameters using:

$$a_s = a_d + \frac{d^2}{0.95p} \tag{1}$$

where d is the diameter of the vias and p is the separation between them along the waveguide propagation direction, see Fig. 2. For these vias to behave as metal walls, they must fulfill the following empirical relations: $d < \lambda_g/5$ and $p \leq 2d$. In this case, we selected $d = 0.5$ mm and $p = 0.7$ mm, which leads to $a_s = 6.19$ mm. The SIW height corresponds to the thickness of the dielectric substrate, which in this case was 508 μm.

Since SIW technology uses a dielectric medium for propagation, it suffers from additional losses compared with other guiding platforms, such as gap-waveguides [13], where air serves as the guiding medium. However, the main advantage of SIW over gap-waveguide-based solutions comes from the simpler and cost-effective manufacturing provided by this technology. In this case, the use of an SIW waveguide allows simple integration with the proposed MTS.

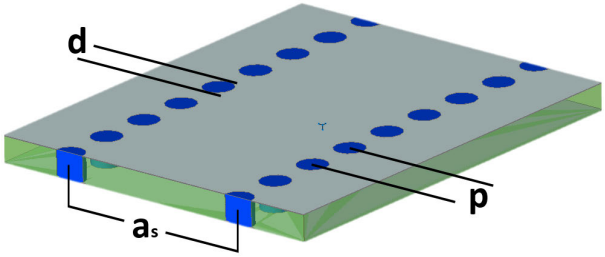

FIGURE 2. SIW model with its design parameters.

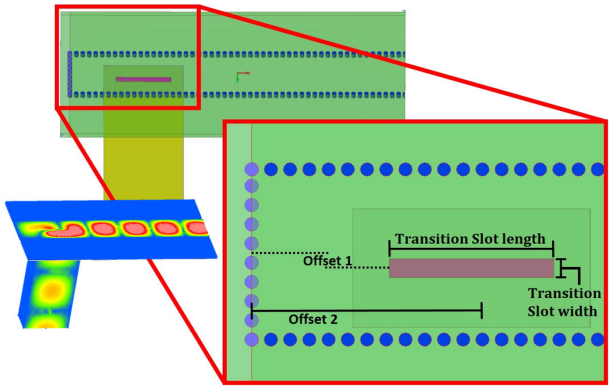

FIGURE 3. WR34 to SIW transition. The top ground plane has been removed to improve the visibility of the coupling slot. The inset shows an snapshot of the electric field distribution along the transition.

In addition, for this frequency range losses are moderate, as shown in the characterization sections.

B. RECTANGULAR WAVEGUIDE TO SIW TRANSITION DESIGN

The SIW antenna was fed using a WR34 rectangular waveguide (8.636 mm × 4.318 mm). In this case, instead of using an inline transition, we opted for a perpendicular configuration [43], since it provides a more compact solution compatible with the layer-by-layer structure of the antenna. Coupling between both waveguides was achieved by means of a slot etched in one of the SIW ground planes.

The transition was optimized by adjusting the coupling slot length and width ("Transition slot length" and "Transition slot width" in Fig. 3) and its position in the transition, i.e. the offset from the waveguide center ("Offset 1") and the distance to the waveguide short-circuit ("Offset 2") to obtain a matching bandwidth ($S_{11} < -10$ dB) broader than that of the antenna, i.e. 4 %. The initial values for the slot length and for the distance between the slot center and the short-circuit were $\lambda_g/2$ and $3\lambda_g/4$, respectively. Once these parameters were optimized, Fig. 4 shows the simulated performance of the transition, where its bandwidth, defined at the 10 dB return loss level, covers the range between 23.5 and 25 GHz, i.e. 6.7 %. Fig. 3. shows the structure of the transition and a snapshot of the electric field distribution across it.

The electrical properties in the working frequency range of the used Rogers RT5880 dielectric substrate were not provided by the manufacturer. To determine them, a WR34-SIW-WR34 back-to-back transition was analyzed

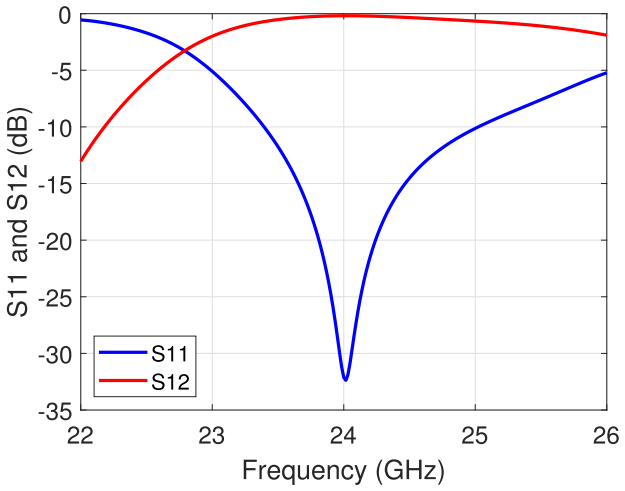

FIGURE 4. Simulated performance of the optimized WR34 to SIW transition.

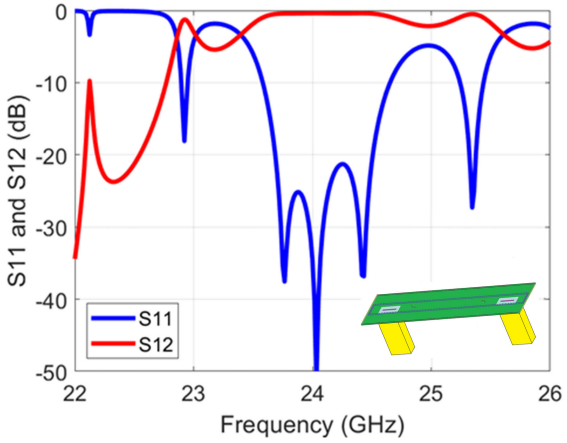

FIGURE 5. Simulation results of the back-to-back WR34-SIW-WR34 transition. The inset shows the back-to-back configuration, where, for improved visibility, the top metal plate and the substrate have been removed.

and tested. The length of the SIW waveguide section in between the two transitions was 74 mm and the two transitions corresponded to the design discussed.

The predicted response of the back-to-back transition is shown in Fig. 5. Besides the reflection minimum at 24 GHz, where each transition is best matched, additional resonances appear because of the mismatch created by the transitions at the ends of the SIW and the SIW section length. These simulation results used ideal metallic ground planes and the nominal value of the loss tangent in the dielectric substrate at 10 GHz, i.e. 0.0009.

This back-to-back transition was not included in the antenna design. However, these results will be used in Section IV, not only to adjust the properties of the dielectric material but also to determine the tolerances of the manufacturing process.

III. ANTENNA DESIGN

The design of the MTS-covered slotted SIW antenna starts by designing an appropriate metasurface, whose response must be centered in the antenna operation band and with periodicity in accordance with the distance between slots. For the antenna design, the standard procedure for slotted waveguide antennas was followed: the positions of the slots were determined such that they were fed with the required amplitudes that create the intended Chebyshev distribution. To this aim, the equivalent conductance model for the radiating slots in a waveguide wall as a function of their distance to the waveguide axis was used. In this case, given the effect of the MTS on the slot radiation, the equivalent conductance was numerically computed. Once these conductance values were available, the required conductance values were converted into slot positions.

TABLE 1. Metasurface parameters. See the inset in Fig. 1 for a reference.

Variable	Description	Values (mm)
h	Dielectric thickness	0.508
t	Width of dipoles and wires	0.27
b	Distance between wires and dipoles	1.67
L_d	Dipole length	3.51
a	Separation between dipoles	4.22

A. METASURFACE DESIGN

The metasurface used in this work is shown in Fig. 1. It consists of a combination of dipoles and a wire grid distributed in three layers [44]. The first and third layers are composed of paired dipoles, and the central one consists of a wire grid, located in between the rows of dipoles, both in the stacking and in-plane directions. For this implementation we used copper strips on the same Rogers RT5880 dielectric substrate used for the SIW. The interlayer spacing was 508 μm, which corresponds to one of the commercial thicknesses of the Rogers RT5880 substrate, and the metal thickness was 17 μm. Table 1 lists the dimensions of the metasurface, which was designed to operate at 24 GHz. These dimensions were adjusted taking into account their compatibility with the wavelength in the SIW, since the separation between the radiating slots is determined by half a wavelength in the SIW. In addition, the thickness of the dielectric substrate was determined by the commercially available standard Rogers RT5880 PCB circuit boards.

Besides the two PCB layers required to hold the dipoles and the grid, two additional PCB boards were used to separate the MTS from the slots and place it at a 1.016 mm distance from the slots. Simulations show that this distance corresponds to a good compromise between excitation of the MTS and impact on the slot radiation performance. Moreover, these additional layers simplify manufacturing of the MTS, since each layer can be printed on a different PCB without requiring a double-sided process. Fig. 1 shows the physical implementation of the MTS and the required four PCB layers.

The MTS analysis was carried out using Ansys HFSS. The MTS unit cell was simulated under plane-wave incidence in a periodic environment. Only the response to the polarization parallel to the dipoles and wires was considered, since this is

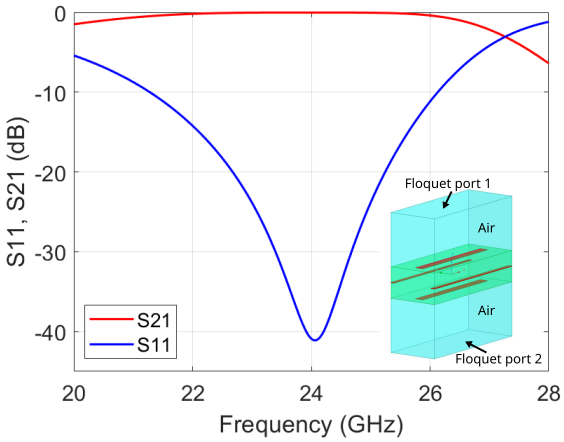

FIGURE 6. Simulated response of the MTS unit cell. Only the response to the polarization parallel to the dipoles is shown. Inset: Set-up used for the analysis of the MTS with Ansys HFSS.

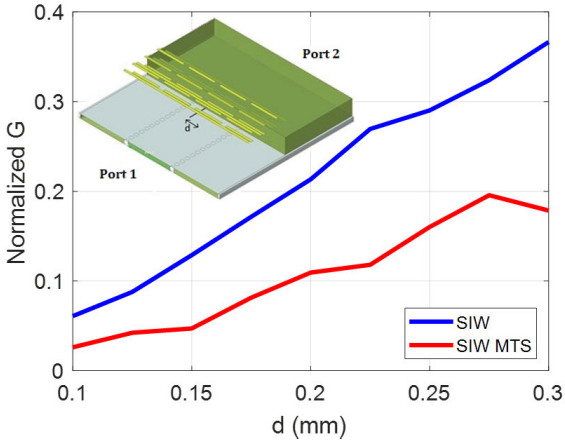

FIGURE 7. Normalized conductance (g) at 24 GHz of a slot in the SIW ground plane. Comparison between MTS-covered SIW and uncovered SIW. Inset: Ansys HFSS model analyzed to obtain the equivalent conductance of a slot in the SIW ground plane, when covered by the MTS. Half of the substrate has been removed to improve visibility.

the one that is affected by the metasurface and is excited by the slots.

This metasurface provides a transmission band around 24 GHz, as shown in Fig. 6. This pass-band relies on the excitation of magnetic dipoles, created by the currents induced in the dipoles and wires. As discussed in [44], within this band the metasurface elements can be excited by a radiating source, in this case the slots. The magnetic dipoles are distributed in a larger area, thereby increasing the effective aperture and gain. Since the MTS mainly increases the radiating aperture in the direction perpendicular to the slots, the principal impact is in the E-plane of the radiation pattern, which narrows. Conversely, the H-plane is predominantly determined by the array of slots and is hardly affected by the metasurface.

B. SLOT CONDUCTANCE

Resonant slotted waveguide antennas can be modelled as shunt admitances, which represent the effect of the slots, connected by $\lambda_g/2$ transmission line sections [45]. This model can be improved for SIW slots by employing a T-network that considers the non-symmetry of the field distribution in the slot [46]. However, in this case the shunt model is sufficient, since the primary objective here is not to achieve precise design accuracy but rather to show the improvements caused by the MTS.

In the case of resonant slots, their conductance is the main design parameter of the slotted waveguide antenna. Therefore, once the dimensions of the SIW and metasurface are determined, the conductance created by a slot in the broadside wall of the SIW must be calculated. This conductance depends on the slot displacement with respect to the waveguide axis and is used to adjust the design to the required slot excitation distribution, following the standard slotted waveguide antenna design procedure. Specifically, our goal is to obtain a Chebyshev distribution with -20 dB sidelobe level.

When working with rectangular waveguide-based slotted arrays, the slot length is close to $\lambda_0/2$ and analytical formulas for the slot conductance can be employed, see e.g. [45]. However, in both SIW arrays and MTS-covered SIW arrays, the equivalent admittance of the slots must be numerically computed. To this end, Ansys HFSS simulations of an SIW section with one slot etched in one of its ground planes were carried out. Since this configuration can be modelled as a shunt admittance in a transmission line, the admittance can be computed from the simulated S_{11} parameter (deembedded to the center of the slot):

$$\frac{Y}{Y_0} = \frac{-2S_{11}}{1+S_{11}} = g + jb \tag{2}$$

where Y_0 is the characteristic admittance of the SIW waveguide.

For the MTS-covered slot admittance calculations, the structure shown in Fig. 7 was used. The slot in the metal plane is covered by 3.5×4 periods of the aforementioned metasurface, in the longitudinal and transversal to the waveguide axis directions. The number of periods in the waveguide longitudinal direction, i.e. 3.5, is determined by the wavelength in the SIW waveguide, whereas the 4 periods in the transversal direction allow to achieve optimum illumination of the MTS. The slot is perpendicular to the MTS dipoles and placed in between the dipoles. This slot orientation provides proper excitation of the metasurface, which requires the radiated electric field to be parallel to the dipoles and wires.

The slot length and its displacement with respect to the waveguide axis were swept, and the equivalent admittance was obtained. Note also that the MTS moves along with the slot, so that the position of the slot with respect to the MTS is the same in all cases. From these results, the slot length for resonant operation, i.e. $b = 0$ in (2), can be determined. Since for the analyzed configurations the displacement of the slot hardly changed its susceptance, all the slots were

TABLE 2. Displacement of the slots with respect to the waveguide axis.

Nº Slot	Distance (mm) with MTS	Distance (mm) without MTS
1 and 8	0.16	0.12
2 and 7	0.18	0.14
3 and 6	0.24	0.18
4 and 5	0.29	0.21
Slot resonant length:	4.7 mm	4.2 mm

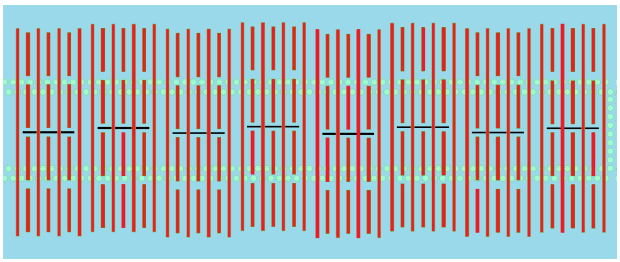

FIGURE 8. Top view of the proposed MTS-covered S-SIW antenna. The dielectric layer has been made semi-transparent to allow visibility of the wire grid and the slots.

considered to have the same length. As a matter of fact, when the slot is covered with the metasurface, due to the MTS loading, the slot resonant length reduces in comparison with the resonant length in the uncovered SIW case: in the MTS-covered configuration the slot resonance length is 4.2 mm, whereas in the slot radiating in air case it is 4.7 mm.

For comparison, the response of a slot on the SIW wall without MTS cover was also obtained. A comparison between these results at 24 GHz is presented in Fig. 7. When the metasurface covers the slot, its conductance is lower, requiring larger displacements of the slot to achieve the same conductance that would be obtained without the use of the metasurface. These low values can limit the design of antennas with a reduced number of slots, which requires high conductance values.

C. ANTENNA DESIGN

Fig. 1 shows a schematic of the different layers that constitute the antenna. Starting from the bottom, the first layer corresponds to the SIW. In its bottom ground plane only the slot used by the rectangular waveguide to SIW transition can be seen. This layer has been detached from the dielectric substrate to improve visibility, although it was physically implemented as one of the ground planes of the SIW layer. This layer, layer 1, is completed by the SIW substrate and top ground plane, where the antenna slots are etched. Layer 2 consists of a non-metalized Rogers RT5880 PCB used as a separation layer, required to have the MTS at a proper distance to the slots, whereas layers 3 to 5 correspond to the MTS: layers 3 and 5 house the dipole pairs, whereas, the wire grid is incorporated in layer 4. The thickness of all PCBs was 0.508 mm.

The proposed design corresponds to a resonant slotted waveguide configuration, where the slots are placed along the waveguide propagation direction, with $\lambda_g/2$ separation [45].

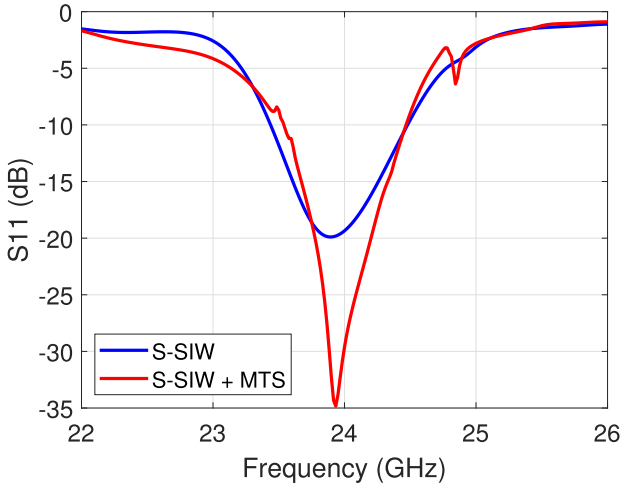

FIGURE 9. Simulated reflection coefficient of the S-SIW antenna with and without metasurface.

The slot positions alternate with respect to the waveguide axis to compensate for the phase changes along the waveguide. The same arrangement was applied to the MTS-covered slotted SIW antenna, where identical MTS sections were placed on top of the slots, as shown in Fig. 8.

In order to obtain the Chebyshev distribution, the conductance results shown in Fig. 7 were used to determine the required slot positions, i.e. their displacements with respect to the SIW axis. These positions are listed in Table 2, corresponding to an 8-element array with 20 dB sidelobe level. Owing to the symmetry of the array, the opposite slots with respect to the array center are located at the same positions with respect to the waveguide axis.

For a comparative analysis, two antennas were designed: one covered by the metasurface and the other without metasurface. As previously discussed, it can be observed that the MTS-covered SIW requires larger slots displacements to achieve the same conductance values. The distance between the slots is the SIW half-wavelength at 24 GHz (6.1 mm) and the distance from the last slot to the SIW short-circuit is a quarter-wavelength (3.05 mm).

D. COMPLETE ANTENNA PERFORMANCE

The matching performance of the two designed antennas is shown in Fig. 9. In both cases the antenna is well matched around the design frequency, 24 GHz, with a similar bandwidth, which is mainly determined by the number of slots.

Regarding the antenna boresight gain, Fig. 10, a 3 dB improvement due to the use of the metasurface can be observed. There is a slight frequency shift between both curves owing to the frequency response of the metasurface, but it does not affect the comparison. In terms of bandwidth, no differences between the antennas can be observed. The antenna operation is constrained by the slotted waveguide configuration, wherein the main beam is divided in the H-plane cut when the frequency deviates significantly from

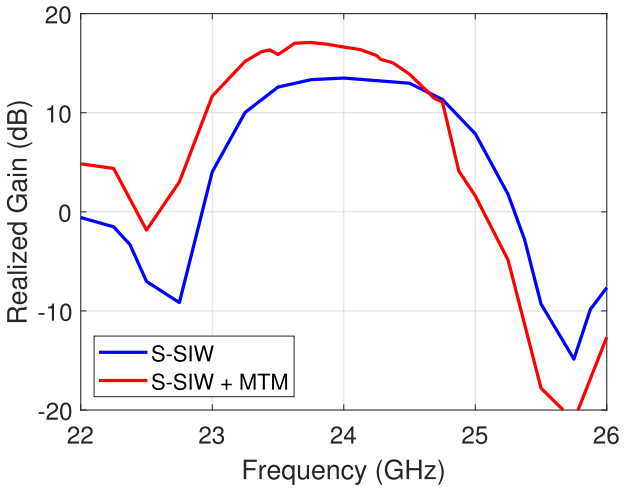

FIGURE 10. Simulated realized gain of the S-SIW antenna with and without metasurface.

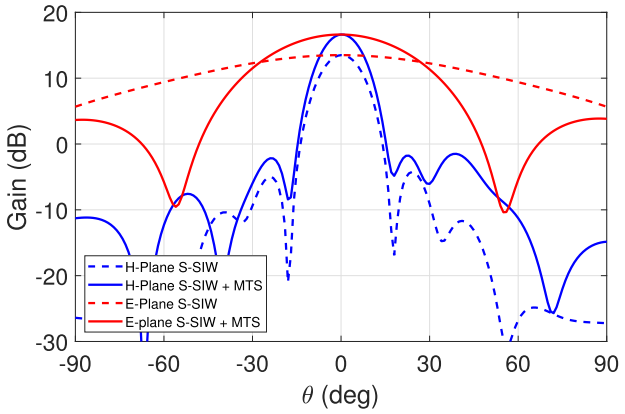

FIGURE 11. Predicted radiation pattern at 24 GHz. Comparison between S-SIW antenna and MTS-covered S-SIW antenna.

the resonant frequency. This phenomenon results in dips occurring at approximately 22.5 and 25.5 GHz, which are common to both antennas.

Fig. 11 shows a comparison of the radiation pattern at 24 GHz between the MTS-covered and uncovered antennas. Slotted waveguide antennas are characterized by an asymmetric pattern, i.e., the radiation pattern E-plane and H-plane are different. The H-plane is dominated by the Chebyshev distribution design. In this plane, the responses of both antennas is very similar and the intended sidelobe level of approximately -20 dB has been achieved.

The main difference between the two designs corresponds to the E-plane. For the uncovered antenna this cut is broad, as it is determined by the slot width. However, when the antenna is covered by the metasurface, the radiating aperture increases in this direction. The metasurface gets nearly uniformly illuminated, allowing to narrow the E-plane pattern. As a consequence, we have a 3 dB increase in gain.

In the previous results, the SIW waveguide was excited by its dominant mode. Using the previously designed transition, a manufacturable antenna fed by a WR34 rectangular

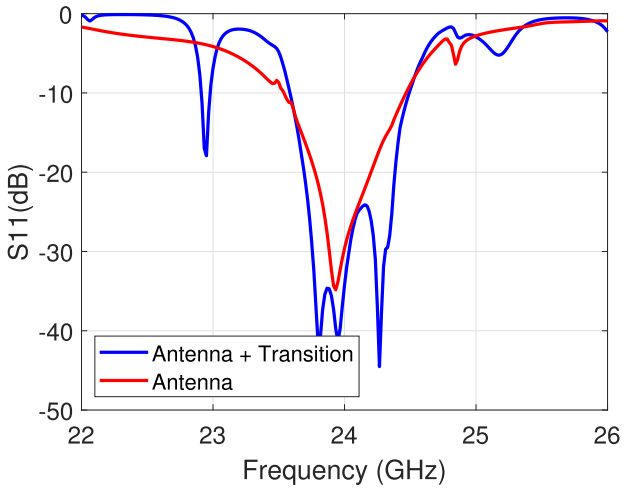

FIGURE 12. Simulated reflection coefficient of the MTS-covered S-SIW antenna with and without transition.

waveguide was designed. The reflection coefficient of the rectangular-waveguide-fed MTS-covered SIW antenna is presented in Fig. 12, where a change in the matching response created by the combination of this transition and the antenna can be seen. The different load caused by the antenna to the transition generates an additional resonance at 23 GHz, which modifies the reflection frequency response. However, the antenna 1-GHz bandwidth around 24 GHz is preserved.

IV. MANUFACTURING AND TEST

A. MANUFACTURING

The fabrication of the antenna involved two processes. On the one hand, the SIW and the metasurface were produced following a standard PCB manufacturing technique. On the other hand, a 6 mm thick metal structure that supports the PCBs and implements the WR34 waveguide was micromachined in aluminum. To simplify manufacturing of this WR34 waveguide section, its corners were rounded with 1 mm radius. This value was already used in the results shown in Fig. 12. Photographs of the different PCB layers of the manufactured prototype are shown in Fig. 13. Due to fabrication tolerances, the dimensions of the manufactured antenna deviated slightly from the nominal design values. A measurement campaign was conducted on the dimensions of the manufactured circuits using the Mitutoyo Hyper MF-U optical measurement microscope, with measurement uncertainty better than $\pm 5\ \mu$m. A comparison between these results is presented in Table 3. The most noteworthy difference corresponds to the diameter of the vias, which is around 0.58 mm instead of the designed 0.5 mm. This parameter determines the width of the SIW and the performance of the WR34-SIW transition and antenna, as discussed in the following sections.

B. TRANSITION CHARACTERIZATION

In addition to the SIW MTS-covered antenna a WR34-SIW-WR34 back-to-back transition was manufactured. The

TABLE 3. MTS-covered slotted SIW antenna dimensions (in mm).

Parameter	Design	Prototype dimensions
MTS dipole width	0.27	0.23
MTS dipole length	3.51	3.38
MTS wire width	0.27	0.24
MTS wire length	16.88	16.6
Slot width	0.1	0.27
Slot length	4.2	4.24
Transition slot width	0.72	0.74
Transition slot length	6	6.02
Vias diameter	0.5	0.58
Distance between vias	0.7	0.62

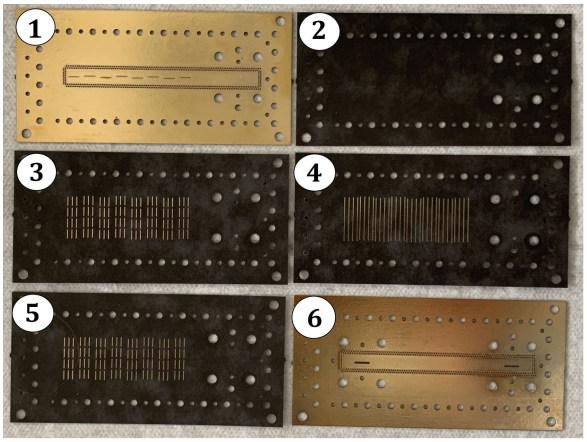

FIGURE 13. Photographs of the different layers of the manufactured prototype: 1: SIW layer, showing the top ground plane, where the slots are etched; 2: Separation layer; 3 and 5: MTS dipole layers; 4: MTS wire grid layer. 6: Photograph of the back-to-back transition.

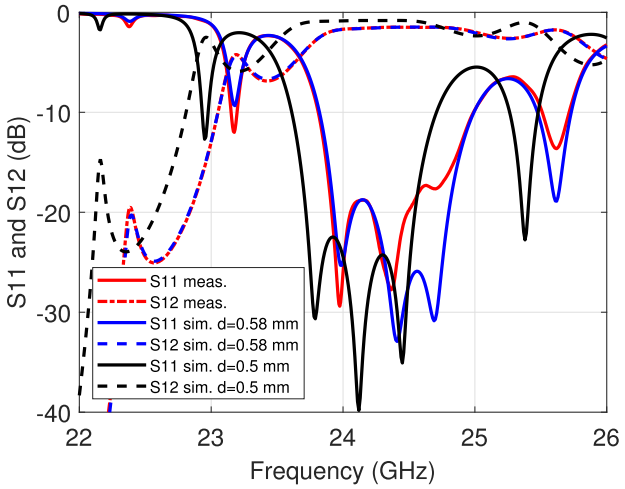

FIGURE 14. Comparison between simulation (nominal and with manufactured dimensions) and measured results of the back-to-back transition.

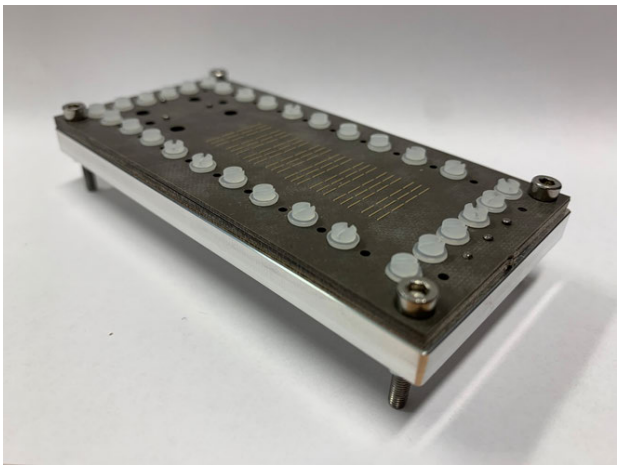

(a)

(b)

FIGURE 15. a) Photograph of the fabricated MTS-covered S-SIW antenna. b) Photograph of the manufactured antenna prototype in the measurement set-up.

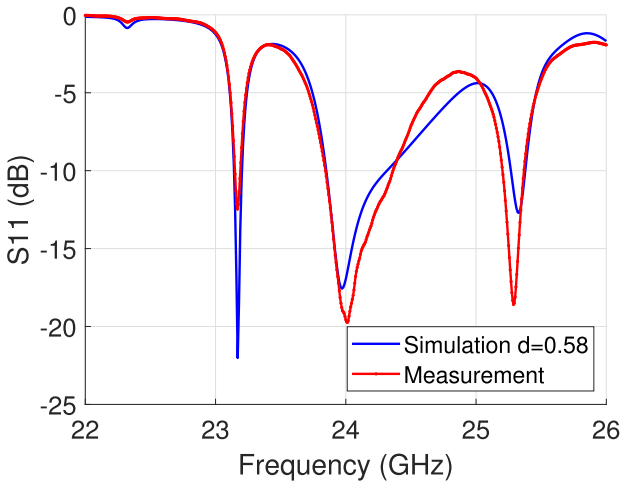

FIGURE 16. Reflection coefficient of the MTS-covered S-SIW. Comparison between simulation (with manufactured dimensions) and measured results of the SIW antenna with the transition and metasurface.

purpose of this component is to help verifying the manufacturing procedure and adjusting certain parameters of the dielectric substrate, such as the loss tangent, which has a significant impact on the antenna performance. A photograph of the back-to-back transition PCB is shown in Fig. 13, 6.

The manufactured back-to-back transition was characterized and the results are presented in Fig. 14. The observed performance is similar to the predictions, but a shift towards higher frequencies can be observed, if both results are compared. In addition, the insertion losses are higher than predicted, due to the higher losses in the substrate and copper cladding.

If the manufactured dimensions are included in the model, a significantly improved agreement is obtained, as shown in Fig. 14. These simulation results incorporate the

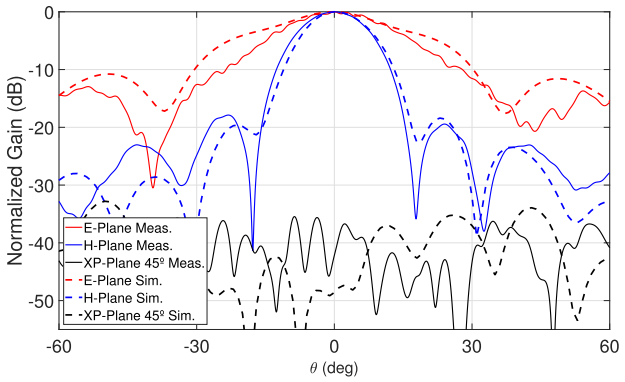

FIGURE 17. Comparison between measured and simulated radiation patterns at 24 GHz of the MTS-covered S-SIW.

TABLE 4. Comparison of the proposed configuration with other MTS-enhanced slot antennas in the literature.

Reference	Bandwidth (GHz)	Thickness	Gain Improvement (dB)
[22]	8.9 - 9.1	0.55 λ_0	1-2
[27]	8.9 - 10.6	0.11 λ_0	3.5
[29]	33.5 - 35.3	3.05 λ_0	6-10
This work	23.7 - 25.0	0.16 λ_0	3

manufactured vias diameter, i.e. 0.58 mm, which shifts the response to higher frequencies. Furthermore, by accounting for additional losses in the dielectric substrate (tanδ=0.0025), as opposed to the nominal value at 10 GHz (tanδ=0.0009), the transmission levels also match the measured response.

C. ANTENNA CHARACTERIZATION

The antenna was assembled and a photograph of the prototype is shown in Fig. 15a. The manufactured antenna was characterized in the Universidad Pública de Navarra's anechoic chamber. The return loss of the antenna is shown in Fig. 16. Similar to the back-to-back transition case, there is a frequency shift in the antenna response, which can be attributed to the thicker vias. When simulations incorporate 0.58 mm diameter vias, the results shown in this figure are in good agreement with the predictions. Besides the frequency shift, the bandwidth is also reduced compared to the nominal design. Our simulations show that this effect can be caused by the presence of air gaps between the metasurface layers. Using 20 μm air gaps in the simulations the resonance at 24.3 GHz (see Fig. 12) disappears, demonstrating good agreement between the simulation and test results.

The antenna pattern was measured in a planar near-field set-up, see Fig. 15b. A near-field to far-field transformation was used to obtain the far-field pattern. Due to the nature of the planar near-field measurement, the measured uncertainty is worse for broader cut-planes. The measured radiation pattern, E-plane, H-plane, and cross-polar components in the 45° cut plane are represented in Fig. 17. A good agreement can be observed between the simulation and measured results. In the E-plane the pattern shows the narrowing effect caused by the metasurface. In the H-plane the results are consistent

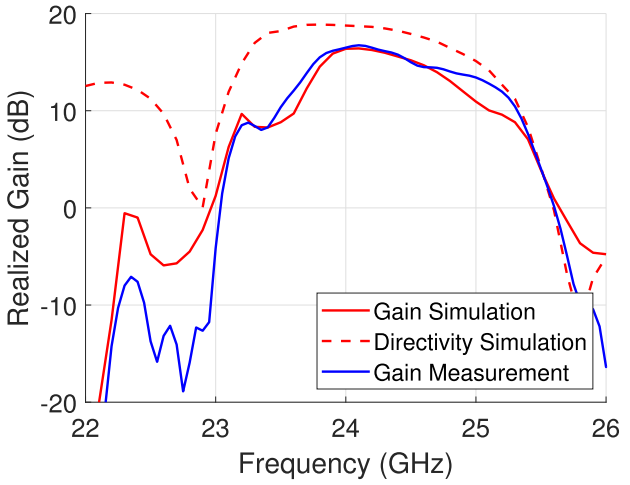

FIGURE 18. Comparison between simulated (with manufactured dimensions) and measured antenna gain and directivity of the MTS-covered S-SIW.

with the intended Chebyshev distribution. However, there is a small asymmetry in the pattern, and one of the sidelobes is slightly lower than -20 dB, whereas the other is marginally higher than the intended design value. This small discrepancy is caused by manufacturing tolerances. Nevertheless, these results are considered satisfactory to demonstrate the main concept of the paper, i.e. the improvements brought about by the use of the metasurface. Finally, the measured cross-polarization levels are similar to the predictions, 30 dB below the maximum of the pattern, showing no effect of the MTS.

The antenna gain was measured using the gain-comparison method. Fig. 18 shows a comparison between the simulation and measured results across frequency. Good agreement between the results is observed. The small discrepancy can be ascribed to the measurement uncertainty, estimated to be approximately $\pm$1 dB and the narrower measured E-plane cut, shown in Fig. 17. The simulated directivity displays a similar trend, and the radiation efficiency in the operational bandwidth is higher than 70 %.

A comparison of our results with those of other MTS-enhanced SIW slot antennas is shown in Table 4. For fair comparison, the results are limited to linear arrays. In these cases the radiating aperture is increased only in the direction perpendicular to the array, leading to 1-2 [22] or 3.5 dB [27] enhancements, similar to the results achieved in this work. The exception to this situation is [29], where the reported gain increase reaches 6 to 10 dB. However, in this case the metasurface acts as a lens, placed at $3\lambda_0$ distance from the array. The need to keep an air gap between the slot and the metasurface also appears in [27]. This complicates manufacturing and assembly and prevents multilayer PCB manufacturing. Consequently, this comparison highlights that although similar gain improvements have been demonstrated in other MTS-enhanced configurations, they may not be compatible with a multilayer PCB manufacturing procedure, as proposed in this paper.

V. CONCLUSION

This study highlights the enhanced performance of a slotted SIW antenna by covering it with a metasurface. In contrast to other solutions that require the metasurface to be separated from the antenna, in this case the metasurface can be placed directly on top of the slotted SIW, preserving the low-profile characteristic inherent to SIW-based antennas. In addition, a perpendicular transition was designed, rendering this compact solution compatible with multilayer PCB manufacturing processes.

The metasurface was adjusted to the limited space available due to the reduced wavelength in the SIW waveguide. The analysis of the equivalent slot conductance reveals the effect of the metasurface, resulting in a decrease in its value. The designed antenna was manufactured and tested. Good agreement with the predictions was obtained and 3 dB gain increase was achieved with respect to a conventional slotted SIW antenna.

Finally, our results demonstrate that the use of a metasurface improves certain characteristics of this type of antennas. The metasurface extends the radiating aperture and narrows the E-plane of the radiation pattern. This type of configuration could be a solution for increasing the radiating aperture of SIW antennas without requiring an array configuration.

REFERENCES

[1] S. Kumar, A. S. Dixit, R. R. Malekar, H. D. Raut, and L. K. Shevada, "Fifth generation antennas: A comprehensive review of design and performance enhancement techniques," *IEEE Access*, vol. 8, pp. 163568–163593, 2020.

[2] E. Garcia-Marin, J. L. Masa-Campos, and P. Sanchez-Olivares, "Planar array topologies for 5G communications in Ku band," *IEEE Antennas Propag. Mag.*, vol. 61, no. 2, pp. 112–133, Apr. 2019.

[3] D. Deslandes and K. Wu, "Integrated microstrip and rectangular waveguide in planar form," *IEEE Microw. Wireless Compon. Lett.*, vol. 11, no. 2, pp. 68–70, Feb. 2001.

[4] D.-F. Guan, C. Ding, Z.-P. Qian, Y.-S. Zhang, W.-Q. Cao, and E. Dutkiewicz, "An SIW-based large-scale corporate-feed array antenna," *IEEE Trans. Antennas Propag.*, vol. 63, no. 7, pp. 2969–2976, Jul. 2015.

[5] P. Chen, W. Hong, Z. Kuai, and J. Xu, "A substrate integrated waveguide circular polarized slot radiator and its linear array," *IEEE Antennas Wireless Propag. Lett.*, vol. 8, pp. 120–123, 2009.

[6] P. Kumar, T. Ali, and M. M. M. Pai, "Electromagnetic metamaterials: A new paradigm of antenna design," *IEEE Access*, vol. 9, pp. 18722–18751, 2021.

[7] C. Milias, R. B. Andersen, P. I. Lazaridis, Z. D. Zaharis, B. Muhammad, J. T. B. Kristensen, A. Mihovska, and D. D. S. Hermansen, "Metamaterial-inspired antennas: A review of the state of the art and future design challenges," *IEEE Access*, vol. 9, pp. 89846–89865, 2021.

[8] M. Faenzi, G. Minatti, D. González-Ovejero, F. Caminita, E. Martini, C. D. Giovampaola, and S. Maci, "Metasurface antennas: New models, applications and realizations," *Sci. Rep.*, vol. 9, no. 1, Jul. 2019, Art. no. 10178.

[9] V. G. Ataloglou, M. Chen, M. Kim, and G. V. Eleftheriades, "Microwave Huygens' metasurfaces: Fundamentals and applications," *IEEE J. Microw.*, vol. 1, no. 1, pp. 374–388, Jan. 2021.

[10] B. A. F. Esmail, S. Koziel, L. Golunski, H. B. A. Majid, and R. K. Barik, "Overview of metamaterials-integrated antennas for beam manipulation applications: The two decades of progress," *IEEE Access*, vol. 10, pp. 67096–67116, 2022.

[11] M. Beruete and I. Jáuregui-López, "Terahertz sensing based on metasurfaces," *Adv. Opt. Mater.*, vol. 8, no. 3, Jul. 2019, Art. no. 26.

[12] M. F. Imani, J. N. Gollub, O. Yurduseven, A. V. Diebold, M. Boyarsky, T. Fromenteze, L. Pulido-Mancera, T. Sleasman, and D. R. Smith, "Review of metasurface antennas for computational microwave imaging," *IEEE Trans. Antennas Propag.*, vol. 68, no. 3, pp. 1860–1875, Mar. 2020.

[13] E. Rajo-Iglesias, M. Ferrando-Rocher, and A. U. Zaman, "Gap waveguide technology for millimeter-wave antenna systems," *IEEE Commun. Mag.*, vol. 56, no. 7, pp. 14–20, Jul. 2018.

[14] O. Quevedo-Teruel, G. Valerio, Z. Sipus, and E. Rajo-Iglesias, "Periodic structures with higher symmetries: Their applications in electromagnetic devices," *IEEE Microw. Mag.*, vol. 21, no. 11, pp. 36–49, Nov. 2020.

[15] G. Minatti, M. Faenzi, E. Martini, F. Caminita, P. De Vita, D. González-Ovejero, M. Sabbadini, and S. Maci, "Modulated metasurface antennas for space: Synthesis, analysis and realizations," *IEEE Trans. Antennas Propag.*, vol. 63, no. 4, pp. 1288–1300, Apr. 2015.

[16] A. Epstein, J. P. S. Wong, and G. V. Eleftheriades, "Cavity-excited Huygens' metasurface antennas for near-unity aperture illumination efficiency from arbitrarily large apertures," *Nature Commun.*, vol. 7, 2016, Art. no. 10360.

[17] M. Bailey, "Design of dielectric-covered resonant slots in a rectangular waveguide," *IEEE Trans. Antennas Propag.*, vol. AP-15, no. 5, pp. 594–598, Sep. 1967.

[18] M. Bailey, "The impedance properties of dielectric-covered narrow radiating slots in the broad face of a rectangular waveguide," *IEEE Trans. Antennas Propag.*, vol. AP-18, no. 5, pp. 596–603, Sep. 1970.

[19] P. B. Katehi, "Dielectric-covered waveguide longitudinal slots with finite wall thickness," *IEEE Trans. Antennas Propag.*, vol. 38, no. 7, pp. 1039–1045, Jul. 1990.

[20] G. A. Casula and G. Montisci, "Design of dielectric-covered planar arrays of longitudinal slots," *IEEE Antennas Wireless Propag. Lett.*, vol. 8, pp. 752–755, 2009.

[21] Z. Jin, G. Montisci, G. Mazzarella, M. Li, H. Yang, and G. A. Casula, "Effect of a multilayer dielectric cover on the behavior of waveguide longitudinal slots," *IEEE Antennas Wireless Propag. Lett.*, vol. 11, pp. 1190–1193, 2012.

[22] G. Montisci, Z. Jin, M. Li, H. Yang, G. A. Casula, G. Mazzarella, and A. Fanti, "Design of multilayer dielectric cover to enhance gain and efficiency of slot arrays," *Int. J. Antennas Propag.*, vol. 2013, pp. 1–6, Sep. 2013.

[23] J.-H. Hwang and Y. Oh, "Millimeter-wave waveguide slot-array antenna covered by a dielectric slab and arrayed patches," *IEEE Antennas Wireless Propag. Lett.*, vol. 8, pp. 1050–1053, 2009.

[24] C. Huang, Z. Zhao, and X. Luo, "The rectangular waveguide board wall slot array antenna integrated with one dimensional subwavelength periodic corrugated grooves and artificially soft surface structure," *J. Infr., Millim., THz Waves*, vol. 30, no. 4, pp. 357–366, Apr. 2009.

[25] D. Garcia-Valverde, J. L. Masa-Campos, P. Sanchez-Olivares, B. Taha-Ahmed, and J. Corcoles, "Linear patch array over substrate integrated waveguide for Ku-band," *IEEE Antennas Wireless Propag. Lett.*, vol. 12, pp. 257–260, 2013.

[26] Y. Liu, H. Yang, Z. Jin, and J. Zhu, "An improvement approach for wide-angle impedance matching using ELC metasurface slabs for SIW slot array antennas," *Int. J. Antennas Propag.*, vol. 2018, pp. 1–8, Jul. 2018.

[27] H. Bai, G.-M. Wang, X.-J. Zou, and T. Wu, "Wideband and gain enhancement SIW slot array antenna using sparsification processing and composite metasurface," *IEEE Trans. Antennas Propag.*, vol. 69, no. 12, pp. 9009–9014, Dec. 2021.

[28] T. Li and Z. N. Chen, "Control of beam direction for substrate-integrated waveguide slot array antenna using metasurface," *IEEE Trans. Antennas Propag.*, vol. 66, no. 6, pp. 2862–2869, Jun. 2018.

[29] M. Chen, A. Epstein, and G. V. Eleftheriades, "Design and experimental verification of a passive Huygens' metasurface lens for gain enhancement of frequency-scanning slotted-waveguide antennas," *IEEE Trans. Antennas Propag.*, vol. 67, no. 7, pp. 4678–4692, Jul. 2019.

[30] M. U. Afzal, K. P. Esselle, and M. N. Y. Koli, "A beam-steering solution with highly transmitting hybrid metasurfaces and circularly polarized high-gain radial-line slot array antennas," *IEEE Trans. Antennas Propag.*, vol. 70, no. 1, pp. 365–377, Jan. 2022.

[31] Y. Liu, Y. Jia, W. Zhang, and F. Li, "Wideband RCS reduction of a slot array antenna using a hybrid metasurface," *IEEE Trans. Antennas Propag.*, vol. 68, no. 5, pp. 3644–3652, May 2020.

[32] J.-W. Lian, D. Ding, and R. Chen, "Wideband millimeter-wave substrate-integrated waveguide-fed metasurface antenna," *IEEE Trans. Antennas Propag.*, vol. 70, no. 7, pp. 5335–5344, Jul. 2022.

[33] S. Pandit, A. Mohan, and P. Ray, "A low-profile high-gain substrate-integrated waveguide-slot antenna with suppressed cross polarization using metamaterial," *IEEE Antennas Wireless Propag. Lett.*, vol. 16, pp. 1614–1617, 2017.

[34] Q. Chen and H. Zhang, "Dual-patch polarization conversion metasurface-based wideband circular polarization slot antenna," *IEEE Access*, vol. 6, pp. 74772–74777, 2018.
[35] Z. H. Jiang, Q. Wu, D. E. Brocker, P. E. Sieber, and D. H. Werner, "A low-profile high-gain substrate-integrated waveguide slot antenna enabled by an ultrathin anisotropic zero-index metamaterial coating," *IEEE Trans. Antennas Propag.*, vol. 62, no. 3, pp. 1173–1184, Mar. 2014.
[36] E. Sáenz, R. Gonzalo, I. Ederra, J. Vardaxoglou, and P. de Maagt, "Highly efficient dipole antenna with planar meta-surface," *Electron. Lett.*, vol. 43, no. 16, pp. 850–852, 2007.
[37] E. Saenz, K. Guven, E. Ozbay, I. Ederra, and R. Gonzalo, "Enhanced directed emission from metamaterial based radiation source," *Appl. Phys. Lett.*, vol. 92, no. 20, May 2008, Art. no. 204103.
[38] E. Saenz, I. Ederra, R. Gonzalo, S. Pivnenko, O. Breinbjerg, and P. de Maagt, "Coupling reduction between dipole antenna elements by using a planar meta-surface," *IEEE Trans. Antennas Propag.*, vol. 57, no. 2, pp. 383–394, Feb. 2009.
[39] J. Chocarro, J. M. P. Escudero, I. Liberal, and I. Ederra, "Metamaterial enhanced slotted waveguide antenna," in *Proc. 11th Int. Congr. Engineered Mater. Platforms Novel Wave Phenomena*, Aug. 2017, pp. 91–93.
[40] J. Chocarro and I. Ederra, "Design of a slotted substrate integrated waveguide antenna using a metasurface," in *Proc. IEEE Int. Symp. Antennas Propag. USNC-URSI Radio Sci. Meeting (APS/URSI)*, Marina Bay Sands, Singapore, Dec. 2021, pp. 879–880.
[41] J. Chocarro, J. M. Pérez-Escudero, and I. Ederra, "Comparison of a slotted SIW antenna covered with metasurface vs. A traditional array," in *Proc. Int. Workshop Antenna Technol. (iWAT)*, Dublin, Ireland, May 2022, pp. 111–113.
[42] D. Deslandes and K. Wu, "Accurate modeling, wave mechanisms, and design considerations of a substrate integrated waveguide," *IEEE Trans. Microw. Theory Techn.*, vol. 54, no. 6, pp. 2516–2526, Jun. 2006.
[43] L. Li, X. Chen, R. Khazaka, and K. Wu, "A transition from substrate integrated waveguide (SIW) to rectangular waveguide," in *Proc. Asia–Pacific Microw. Conf.*, Dec. 2009, pp. 2605–2608.
[44] P. M. T. Ikonen, E. Saenz, R. Gonzalo, and S. A. Tretyakov, "Modeling and analysis of composite antenna superstrates consisting on grids of loaded wires," *IEEE Trans. Antennas Propag.*, vol. 55, no. 10, pp. 2692–2700, Oct. 2007.
[45] R. Elliott, "An improved design procedure for small arrays of shunt slots," *IEEE Trans. Antennas Propag.*, vol. AP-31, no. 1, pp. 48–53, Jan. 1983.
[46] S. Sheel and J. C. Coetzee, "Compensation for asymmetrical slot fields in the design of SIW slot arrays," in *Proc. IEEE Int. Conf. Microw., Antennas, Commun. Electron. Syst. (COMCAS)*, Tel-Aviv, Israel, Nov. 2019, pp. 1–4.

JAVIER CHOCARRO (Student Member, IEEE) was born in Pamplona, Spain, in 1995. He received the M.Sc. degree in telecommunication engineering from the Universidad Pública de Navarra, in 2019, where he is currently pursuing the Ph.D. degree.

His research interests include slotted waveguide antennas and the application of metasurfaces for antennas.

JOSÉ MANUEL PÉREZ-ESCUDERO was born in Murcia, Spain, in 1988. He received the degree in telecommunication engineering from the Universidad Politécnica de Cartagena, Murcia, in 2014, and the Ph.D. degree in telecommunication engineering from the Universidad Pública de Navarra, Pamplona, Spain, in 2019.

From September 2013 to March 2014, he was with the Fraunhofer Institute for High Frequency Physics and Radar Techniques, Bonn, Germany, where he was working on waveguide and planar technology filters and their applications in radar systems. Since April 2015, he has been with the Antenna Group, Department of Electrical, Electronic and Communications Engineering, Universidad Pública de Navarra. His research interests include terahertz components, antennas, and their applications.

JORGE TENIENTE was born in Lodosa, Navarra, Spain, in 1973. He received the M.Sc. and Ph.D. degrees in telecommunication engineering from the Universidad Pública de Navarra (UPNA), Pamplona, Spain, in 1997 and 2003, respectively.

Since 1997, he has been with the Antenna Group, UPNA, where he is currently an Associate Professor. From 1999 to 2000, he was a Spanish Trainee with the European Space Agency (ESA)/ESTEC, Noordwijk, The Netherlands. In Summer 2002, he was a Research Scientist with the ESA Project "StarTiger 1," Rutherford Appleton Laboratory, Chilton, Didcot, U.K. From 2004 to 2005, he was with the University of Oviedo, Asturias, Spain. During his research activity, he has designed antennas for various satellites, radiometers, radio telescopes, and various related applications for more than 25 years. He is a Founding Partner of company Anteral S.L., Pamplona, Navarra, which markets high-performance horn antennas for space and ground applications; low-cost radar products; and components/technologies in the microwave, millimeter, submillimeter, and THz frequency bands. His current area of research is in the field of horn antenna technology; orthomode transducers (OMTs); septums and polarizers; design, manufacture, and measurement of horn antennas in mm-wave, sub-mm-wave, and THz frequencies; and fabrication of mm-wave and sub-mm-wave circuits at clean room environment.

Dr. Teniente received the Second Prize Award of the V. Rosina Ribalta Awards, in 2003; and the Telefónica Foundation Award at the XXIV Awards of Colegio Oficial de Ingenieros de Telecomunicación (COIT) and Asociación Española de Ingenieros de Telecomunicación (AEIT), in 2004.

JUAN CARLOS IRIARTE-GALARREGUI received the Ingeniero de Telecomunicación and Ph.D. degrees from the Universidad Pública de Navarra (UPNA), Pamplona, Spain, in 2002 and 2008, respectively.

In July 2001, he joined the Antennas Group, Electrical, Electronic and Communications Engineering Department, UPNA. Since 2022, he has been an Associate Professor with UPNA. He was a Co-Founder of the spin-off company Anteral S.L., Pamplona, where he is a member of the Advisory Board. He has involved in 90 research projects and contracts with different companies, acting as a project manager in 16. He has 20 journal publications and 92 conference papers. He has coauthored three book chapters. His current research interests include THz sensing and the application of metamaterials to antennas, with an emphasis on space antenna applications, the agri-food industry, and RCS reduction.

IÑIGO EDERRA (Member, IEEE) received the M.Sc. and Ph.D. degrees in telecommunication engineering from the Universidad Pública de Navarra, Pamplona, Spain, in 1996 and 2004, respectively.

In 1997, he joined the Microwave and Millimetre Wave Group, Universidad Pública de Navarra. From 1999 to 2000, he was with the European Space Research and Technology Centre (ESTEC), ESA, Noordwijk, The Netherlands, where he was working on electromagnetic bandgap materials and their applications in the field of antennas. Since 2001, he has been with the Antenna Group, Universidad Pública de Navarra, where he has been a Leader, since 2012. From June 2002 to October 2002, he was a Visitor Scientist with the Rutherford Appleton Laboratory, Chilton, Didcot, U.K., participating in ESA's Startiger I Project. Since 2022, he has been a Full Professor with the Universidad Pública de Navarra, where he is a member of its Institute of Smart Cities. His research interests include metamaterials and metasurfaces and their applications in microwave, millimeter-wave, and THz components and antennas.